Biointerface Research in Applied Chemistry
Open-Access Journal (ISSN: 2069-5837)

Article
Volume 14, Issue 6, 2024, 128
https://doi.org/10.33263/BRIAC146.128

Numerical Study of MHD Ternary Hybrid Nanofluid (Ag-$CoFe_2O_4$-ZnO/$C_2H_6O_2$+H_2O): Effects of Thermal Stratification on a Vertical Stretching Cylinder in a Porous Environment

Digbash Sahu [1,*], Rudra Kanta Deka [1]

[1] Department of Mathematics, Gauhati University, Guwahati-781014, Assam, India; digbashsahu79@gmail.com (D.S.); rkdgu@gauhati.ac.in (R.K.D.);
* Correspondence: digbashsahu79@gmail.com;

Scopus Author ID 59172195500
Received: 19.07.2024; Accepted: 6.10.2024; Published: 10.12.2024

Abstract: This study explores the impact of thermal stratification on the magnetohydrodynamic flow of ethylene glycol and water-based nano, hybrid, and ternary hybrid nanofluids past a vertically stretching cylinder beneath a porous medium. Composed of silver (Ag), cobalt ferrite ($CoFe_2O_4$), and zinc oxide (ZnO) nanoparticles suspended in a mixture of ethylene glycol ($C_2H_6O_2$) and water (H_2O), the ternary hybrid nanofluid is examined. The governing boundary layer equations are transformed into nonlinear ordinary differential equations using similarity variables and solved using the 3-stage Lobatto IIIa method via the bvp4c solver in MATLAB. The study assesses the effects of dimensionless parameters such as prandtl number, heat source/sink, magnetic, porosity, curvature, thermal stratification, and thermal buoyancy on velocity and temperature profiles, skin friction coefficient, and local Nusselt number. Results indicate that velocity decreases with increases in δ, M, and K and increases with λ. Temperature decreases with increases in δ and Pr, yet rises with Q. Skin friction is boosted by λ and Q but reduced by δ, M, K, Pr, and γ. The local Nusselt number increases with λ, Pr, and γ, but decreases with δ, M, K, and Q. The ternary hybrid nanofluid displays enhanced heat transfer rates and greater absolute skin friction compared to both hybrid and conventional nanofluids, highlighting the significant influence of thermal stratification on MHD ternary hybrid nanofluid flow.

Keywords: bvp4c; MHD; porous medium; thermal radiation; thermal stratification; ternary hybrid nanofluid; vertical stretching cylinder;

1. Introduction

Ternary hybrid nanofluids are specialized fluids comprising three distinct types of nanoparticles dispersed within a base fluid. This paper presents a numerical investigation into an MHD ternary hybrid nanofluid comprised of silver (Ag), cobalt ferrite ($CoFe_2O_4$), and zinc oxide (ZnO) nanoparticles, which are evenly distributed in a blend of ethylene glycol ($C_2H_6O_2$) and water (H_2O). This ternary hybrid nanofluid possesses unique properties that render it appropriate for various uses. The inclusion of silver (Ag) nanoparticles in the nanofluid has been demonstrated to improve thermal conductivity, while the inclusion of cobalt ferrite ($CoFe_2O_4$) and zinc oxide (ZnO) nanoparticles enhances heat transfer effectiveness and stability. This nanofluid can be used in multiple areas, including heat exchangers, cooling systems, and electronic devices, with the aim of enhancing heat dissipation and improving thermal management. Silver nanoparticles exhibit antibacterial properties, while ZnO nanoparticles exhibit photocatalytic action against bacteria. The use of the ternary hybrid nanofluid, comprising Ag−$CoFe_2O_4$−ZnO, presents a promising approach for developing antimicrobial coatings on different surfaces, such as medical devices, fabrics, and food containers. These coatings successfully inhibit bacterial growth and help in preserving cleanliness. Zinc oxide (ZnO) nanoparticles have photocatalytic properties, enabling the degradation of organic pollutants and the purification of water. The utilization of the Ag−$CoFe_2O_4$−ZnO ternary hybrid nanofluid shows potential in thermal conductivity, heat transfer effectiveness, antibacterial properties, and photocatalytic activity, rendering it suitable for cooling systems, antibacterial coatings, and water treatment processes, assisting in the removal of pollutants and enhancing the overall quality of water resources.

The idea of nanofluid, originally proposed by scientists, revolutionized fluid dynamics with nanoparticles. The concept of nanofluid was first introduced by Choi[1], suggesting that heat transfer fluids containing metallic nanoparticles could revolutionize heat transfer fluids. In groundbreaking studies, Das *et al*. [2] and [3] explored the natural convective flow of nanofluids with radiation in a moving vertical plate and a vertical channel, respectively. Both investigations examined water-based nanofluids composed of titanium dioxide, aluminum oxide, and copper. Addressing heat production or absorption scenarios, Rashidi *et al*. [4] sought a Lie group solution for the flow of nanofluid over a chemically reacting horizontal plate. The entropy analysis by Abolbashari *et al.* [5] employed the Homotopy Analysis Method (HAM) to examine a nanofluid composed of water and one of four distinct types of nanoparticles: TiO_2, Al_2O_3, Cu, and CuO, passing across a stretchable permeable surface. In a numerical study, Motsumi *et al.* [6] focused on the boundary layer movement of nanofluids over a moving flat plate, specifically the impacts of thermal radiation, viscous dissipation, and thermal diffusion. Considering velocity slip and temperature jump conditions, Turkyilmazoglu[7] conducted an analytical study on MHD nanofluid flow using various water-based nanoparticles across a continuously stretching/shrinking permeable sheet.

Further, Sahu and Deka [8] explored the stratifications in a MHD parabolic flow with periodic temperature variation and variable mass diffusion in a porous medium. In addition, Cheng [9] and [10] investigated double-diffusive natural convection and combined heat and mass transfer in non-Newtonian fluid-saturated porous media with thermal and mass stratification. In their theoretical analyses, recent studies by Sahu et al. [11–17] focused on thermal and mass stratification effects on MHD flow with variable temperature and mass diffusion, including chemical reactions, heat sources, and thermal radiation. The impact of nanoparticle shape on heat transfer enhancement in magnetized ternary hybrid nanofluid was explored by Shanmugapriya *et al*. [18]. Arif *et al*. [19] investigated heat transfer in a radiator with differently shaped nanoparticles in a water-based ternary hybrid nanofluid, utilizing a fractional model. Finally, Patil *et al*. [20] explored the flow of tangent hyperbolic ternary hybrid nanofluid over a rough-yawed cylinder due to impulsive motion. Mahmood *et al*. [21] examined the effects of suction and a heat source on ternary hybrid nanofluid's MHD stagnation point flow over a convectively heated cylinder.

Additionally, Cao *et al*. [22] simulated the dynamics of water-based colloidal mixtures with various nanoparticles, focusing on ternary-hybrid nanofluids. Recent numerical investigations by Nath *et al*. [23] and [24] delved into the MHD ternary hybrid nanofluid (Cu-Al_2O_3-TiO_2/H_2O) flowing past a vertically stretching cylinder within a porous medium influenced by thermal stratification, analyzing the effects of radiation and thermal stratification.

Sarma and Paul [25] studied thermophoresis and Brownian motion in bioconvective cylindrical-shaped Ag–CuO/H_2O Ellis hybrid nanofluid flow along a radiative stretched tube with an inclined magnetic field. Paul *et al*. [26] examined the mixed convection of shear-thinning hybrid nanofluid flow across a radiative unsteady cone with suction and slip effects. Paul et al. [27] also explored thermal and mass transfer analysis of Casson-Maxwell hybrid nanofluids through an unsteady horizontal cylinder with variable thermal conductivity and Arrhenius activation energy.

According to the literature review, previous research has not addressed the MHD ternary nanofluid (Ag−$CoFe_2O_4$−ZnO/$C_2H_6O_2$ + H_2O) flowing via a porous substance past a cylinder that is extending vertically. The primary aim of this research is to investigate the heat transfer attributes of a ternary hybrid nanofluid comprising Ag−$CoFe_2O_4$−ZnO particles dispersed in ethylene glycol and water. The bvp4c technique applied in this study is well-established, as discussed and applied in MATLAB by Shampine *et al*. [28] and Kierzenka *et al*. [29]. Graphical representation results are given for various parameters, such as δ, γ, M, K, Q, Pr, and λ.

2. Mathematical Analysis

Envision a two-dimensional steady incompressible ternary hybrid nanofluid consisting of Ag−$CoFe_2O_4$−ZnO/$C_2H_6O_2$+H_2O, flowing through a porous medium around a vertically stretchable cylinder with a radius of r_0. Influences on this system include a heat source/sink, thermal stratification, and thermal radiation. The movement of the ternary hybrid nanofluid is directed axially along the x-direction, with the radial coordinate r perpendicular to the x-axis, as depicted in Figure 1. The velocity components of the nanofluid along the r and x axes are denoted by "u" and "v", respectively. A magnetic field with strength B_0 is applied perpendicularly to the flow. The study accounts for thermal buoyancy effects but excludes Joule heating. The velocity that causes the cylinder to stretch linearly is defined as $u = a\frac{x}{l}$, where 'a' is the velocity coefficient and 'l' the characteristic length of the cylinder. The wall temperature varies as $T_w(x) = T_0 + A(\frac{x}{l})$ and the ambient temperature of the nanofluid as $T_\infty(x) = T_0 + B(\frac{x}{l})$, with A, B, and T0 being constants where T_0 indicates the initial temperature. The governing equations for continuity, momentum, and energy for the ternary hybrid nanofluid are outlined according to Paul *et al*. [30].

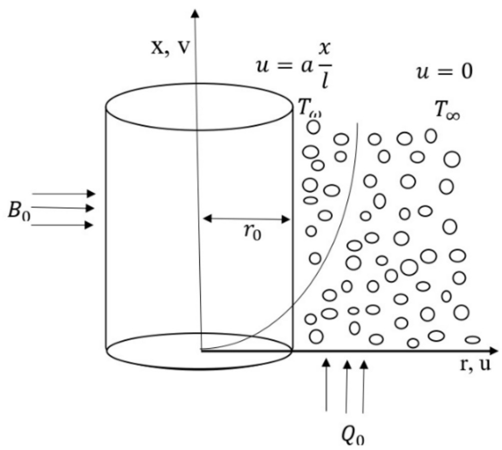

Figure 1. Physical model.

$$\frac{\partial(ru)}{\partial x} + \frac{\partial(rv)}{\partial r} = 0 \quad (1)$$

$$u\frac{\partial u}{\partial x} + v\frac{\partial u}{\partial r} = \frac{\mu_{mnf}}{\rho_{mnf}}\frac{1}{r}\frac{\partial}{\partial r}\left(r\frac{\partial u}{\partial r}\right) + \frac{(\rho\beta_T)_{mnf}}{\rho_{mnf}}g(T - T_\infty) - \frac{\sigma_{mnf}}{\rho_{mnf}}B_0^2 u - \frac{\mu_{mnf}}{\rho_{mnf}}\frac{u}{k'} \quad (2)$$

$$u\frac{\partial T}{\partial x}+v\frac{\partial T}{\partial r}=\frac{k_{mnf}}{(\rho c_p)_{mnf}}\frac{1}{r}\frac{\partial}{\partial r}\left(r\frac{\partial T}{\partial r}\right)+\frac{Q_0}{(\rho c_p)_{mnf}}(T-T_\infty) \quad (3)$$

The boundary conditions are specified as follows:

u = $a\frac{x}{l}$, v = 0, T = $T_w(x)$, when r = r_0

u = 0, T → $T_\infty(x)$, when r → ∞

The similarity transformation (Ref. [30]) applied to Equations (1)-(3) is as follows.

$$\eta=\frac{r^2-r_0^2}{2r_0}\sqrt{\frac{a}{\nu_f l}},\ \psi=\sqrt{\frac{a\nu_f}{l}}xr_0 f(\eta),\ \theta=\frac{T-T_\infty(x)}{T_w(x)-T_0}$$

The non-dimensional quantities are provided as follows:

$$M=\frac{l\sigma_f B_0^2}{a\rho_f},\ K=\frac{l\nu_f}{ak},\ \gamma=\sqrt{\frac{l\nu_f}{ar_0^2}},\ \lambda=\frac{Gr}{Re_x^2},\ \delta=\frac{B}{A},\ Q=\frac{Q_0 l}{a(\rho c_p)_f},\ Pr=\frac{\nu_f(\mu c_p)_f}{k_f}$$

Where δ represents thermal stratification, γ curvature, M magnetism, λ thermal buoyancy, K porosity, Q heat source/sink, and P r the Prandtl number.

To meet the requirements of the continuity equation (1), the stream function ψ is introduced, with $u=\frac{1}{r}\frac{\partial\psi}{\partial r}$ and $v=-\frac{1}{r}\frac{\partial\psi}{\partial x}$. Consequently, the dimensionless versions of the transformed equations are displayed as follows:

$$f'^2-ff''=a_1[2\gamma f''+(1+2\gamma\eta)f''']+a_2\lambda\theta-(a_3M+a_1K)f' \quad (4)$$

$$f'(\theta+\delta)-f\theta'=a_4[2\gamma\theta'+(1+2\gamma\eta)\theta'']+a_5 \quad (5)$$

Where,

$$x_1=\frac{\mu_{mnf}}{\mu_f},\ x_2=\frac{\rho_f}{\rho_{mnf}},\ x_3=\frac{(\rho\beta_T)_{mnf}}{(\rho\beta_T)_f},\quad x_4=\frac{(\rho C_p)_f}{(\rho C_p)_{mnf}},\quad x_5=\frac{\sigma_{mnf}}{\sigma_f},x_6=\frac{k_{mnf}}{k_f}$$

$$a_1=x_1x_2,\quad a_2=x_2x_3,\quad a_3=x_2x_5,\quad a_4=\frac{x_4x_6}{Pr},\quad a_5=Qx_4$$

Here, the variables μ_{mnf}, $(\beta T)_{mnf}$, ρ_{mnf}, $(\rho C_p)_{mnf}$, k_{mnf}, σ_{mnf} refer to the viscosity, thermal expansion coefficient, electrical conductivity, heat capacity, thermal conductivity, and density of the ternary hybrid nanofluid, respectively. In a similar manner, μ_f, $(\beta T)_f$, ρ_f, $(\rho Cp)_f$, k_f, σ_f correspond to the viscosity, thermal expansion coefficient, electrical conductivity, heat capacity, thermal conductivity, and density of the base fluid, respectively.

Here is how the transformed boundary conditions are defined:

$$f(\eta)=0,\quad f'(\eta)=1,\quad \theta(\eta)=1-\delta\quad \text{at } \eta=0$$

$$f'(\eta)\to 0,\quad \theta(\eta)\to 0\quad \text{at } \eta\to\infty$$

The thermophysical properties [Table 1] of the ternary hybrid nanofluid are as follows:

$$\mu_{mnf}=\frac{\mu_f}{(1-\phi_1)^{2.5}(1-\phi_2)^{2.5}(1-\phi_3)^{2.5}}$$

$$\rho_{mnf}=(1-\phi_3)[(1-\phi_2)\{(1-\phi_1)\rho_f+\phi_1\rho_{s1}\}+\phi_2\rho_{s2}]+\phi_3\rho_{s3}$$

$$(\rho c_p)_{mnf}=(1-\phi_3)\left[(1-\phi_2)\left\{(1-\phi_1)(\rho c_p)_f+\phi_1(\rho c_p)_{s1}\right\}+\phi_2(\rho c_p)_{s2}\right]+\phi_3(\rho c_p)_{s3}$$

$$(\rho\beta_T)_{mnf}=(1-\phi_3)[(1-\phi_2)\{(1-\phi_1)(\rho\beta_T)_f+\phi_1(\rho\beta_T)_{s1}\}+\phi_2(\rho\beta_T)_{s2}]+\phi_3(\rho\beta_T)_{s3}$$

$$k_{nf}=\left[\frac{(k_{s1}+2k_f)-2\phi_1(k_f-k_{s1})}{(k_{s1}+2k_f)+\phi_1(k_f-k_{s1})}\right]k_f,\quad k_{hnf}=\left[\frac{(k_{s2}+2k_{nf})-2\phi_2(k_{nf}-k_{s2})}{(k_{s2}+2k_{nf})+\phi_2(k_{nf}-k_{s2})}\right]k_{nf}$$

$$k_{mnf}=\left[\frac{(k_{s3}+2k_{hnf})-2\phi_3(k_{hnf}-k_{s3})}{(k_{s3}+2k_{hnf})+\phi_3(k_{hnf}-k_{s3})}\right]k_{hnf},\quad \sigma_{nf}=\left[\frac{(\sigma_{s1}+2\sigma_f)-2\phi_1(\sigma_f-k_{s1})}{(\sigma_{s1}+2\sigma_f)+\phi_1(\sigma_f-\sigma_{s1})}\right]\sigma_f,$$

$$\sigma_{hnf}=\left[\frac{(\sigma_{s2}+2\sigma_{nf})-2\phi_2(\sigma_{nf}-\sigma_{s2})}{(\sigma_{s2}+2\sigma_{nf})+\phi_2(\sigma_{nf}-\sigma_{s2})}\right]\sigma_{nf},\quad \sigma_{mnf}=\left[\frac{(\sigma_{s3}+2\sigma_{hnf})-2\phi_3(\sigma_{hnf}-\sigma_{s3})}{(\sigma_{s3}+2\sigma_{hnf})+\phi_3(\sigma_{hnf}-\sigma_{s3})}\right]\sigma_{hnf}$$

Here, φ_1, φ_2, and φ_3 signify the volume fractions of Ag (silver), $CoFe_2O_4$ (cobalt ferrite), and ZnO (zinc oxide) nanoparticles, correspondingly. The designations mnf, hnf, nf, f, s1, s2, and s3 refer to ternary hybrid nanofluid, hybrid nanofluid, nanofluid, base fluid, and the dense nanoparticles of Silver (Ag), Cobalt ferrite ($CoFe_2O_4$), and Zinc Oxide (ZnO), respectively.

The definitions of the skin friction coefficient and local Nusselt number are as follows:

$$C_f Re_x^{1/2} = \frac{1}{(1-\phi_1)^{2.5}(1-\phi_2)^{2.5}(1-\phi_3)^{2.5}} f''(0) \text{ and } Nu_x Re_x^{-1/2} = -\frac{k_{mnf}}{k_f}\theta'(0)$$

where Re_x represents the local Reynolds Number.

Table 1. Thermal and physical properties of ethylene glycol+ water and nanoparticles Paul *et al*. [31] and [32].

Physical Properties	**Ethylene glycol (30%)+ H_2O (70%)**	**Ag**	**$CoFe_2O_4$**	**ZnO**
ρ (kg/m^3)	1038.0	10500	4907.0	5606
C_p (J/kgK)	3714.0	235	700.0	544
k (W/mK)	0.484	429	3.7	19

3. Method of Solution

To put it numerically tackle the system of higher-order nonlinear ODEs outlined in Equations (4)-(5) along with the associated boundary circumstances, (6), we employ the bvp4c solver, which is integrated into the MATLAB computational environment. This method is frequently used by both professionals and researchers to analyze fluid flow dynamics. Developed by Jacek Kierzenka and Lawrence F. Shampine from Southern Methodist University in Texas, the bvp4c solver was first introduced by Hale [33]. It utilizes a finite modification algorithm alongside the Lobatto IIIA implicit Runge-Kutta method, delivering numerical solutions with fourth-order accuracy. This method is crucial for ensuring precision by allowing for initial guesses at mesh points and adjustments in step size. In research conducted by Waini *et al*. [34], the bvp4c solver was shown to yield satisfactory outcomes when compared to the shooting technique and the Keller box method. To manage the greater-order derivatives concerning η, we introduce the following new variables:

$$f = y(1), \quad f' = y(2), \quad f'' = y(3), \quad \theta = y(4), \quad \theta' = y(5)$$

$$\frac{d}{d\eta}\begin{bmatrix} y(1) \\ y(2) \\ y(3) \\ y(4) \\ y(5) \end{bmatrix} = \begin{bmatrix} y(2) \\ y(3) \\ \frac{y(2)^2 - y(1)y(3) - a_2\lambda y(4) + (a_3 M + a_1 K)y(2) - 2a_1\gamma y(3)}{(1+2\gamma\eta)a_1} \\ y(5) \\ \frac{y(2)(y(4)+\delta) - y(1)y(5) - 2a_4\gamma y(5) - a_5 y(4)}{(1+2\gamma\eta)a_4} \end{bmatrix}$$

The boundary conditions are stated as:

$$ya(1), \quad ya(2) - 1, \quad ya(4) - 1 + \delta, \quad yb(2), \quad yb(4)$$

Where ya represents the state at $\eta = 0$, and yb denotes the state at $\eta = \infty$.

4. Results and Discussion

The figures analyses were conducted using the bvp4c solver in MATLAB, with findings depicted in Figures 2-13 and Tables 3-5. Table 2 contrasts the values of $-\theta'(0)$ derived from this research with those previously stated by Ishak and Nazar [35] and Elbashbeshy *et al*. [36] when no nanoparticle volume fractions are present and the parameters $\delta = \gamma = M = K = Q = \lambda = \varphi_1 = \varphi_2 = \varphi_3 = 0$, with varying values of the Prandtl number. This comparison validates that the bvp4c algorithm can produce numerical results that are precise and consistent with those obtained from other methodologies.

Table 2. Comparable values of $-\theta'(0)$ with $\delta = \gamma = M = K = Q = \lambda = \varphi_1 = \varphi_2 = \varphi_3 = 0$.

Pr	Ishak and Nazar [35]	Elbashbeshy *et al.* [36]	Present Study
1	1.0	1.0	0.9999
10	3.7207	3.7207	3.7213

The study uses the following values: $\delta = 0.4$, $\gamma = 0.3$, $M = 1.3$, $K = 3$, $Q = 0.3$, $\lambda = 1.5$, $Pr = 6.2$, $\varphi_1 = 0.03$, $\varphi_2 = 0.10$ and $\varphi_3 = 0.15$. Figure 2 illustrates the effect of the thermal stratification (δ) parameter on the velocity $f'(\eta)$. As thermal stratification (δ) intensifies, it leads to a decrease in velocity. An escalation in the thermal stratification (δ) parameter reduces the effective convective interaction between the heated wall and the adjacent fluid, reducing the buoyancy force and consequently slowing the flow velocity. Illustrated in Figure 3, the fluid velocity $f'(\eta)$ falls as the magnetic parameter (M) increases. The increase in (M) leads to a thinner momentum boundary layer due to the Lorentz force exerted by the horizontal magnetic field, which diminishes the velocity of the ternary hybrid nanofluid. Figure 4 shows how the porosity parameter (K) affects the nanofluid velocity $f'(\eta)$. With an increase in (K), the velocity decreases. An inverse correlation exists between K and the porous medium's diameter, where a higher K corresponds to a decreasing diameter. This smaller diameter restricts fluid movement via the porous medium, reducing velocity due to the resistance posed by the porosity parameter (K).

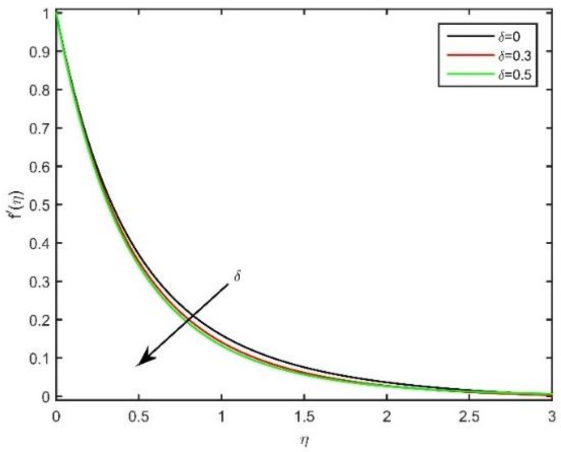

Figure 2. Effects of δ on the velocity profile.

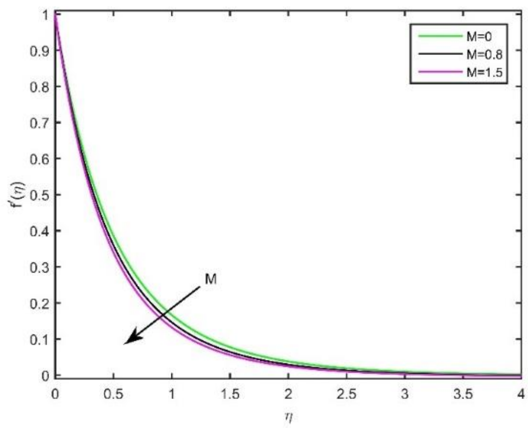

Figure 3. Effects of M on the velocity profile.

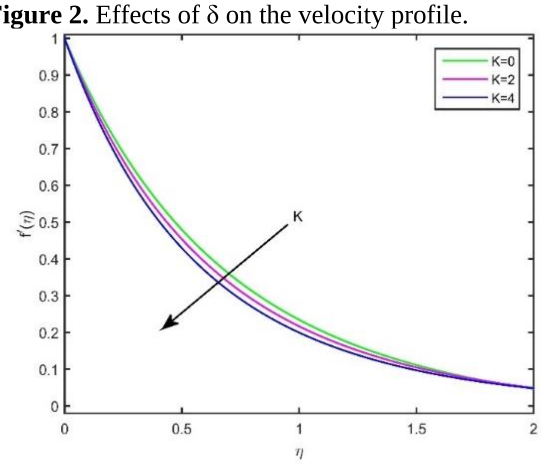

Figure 4. Effects of K on the velocity profile.

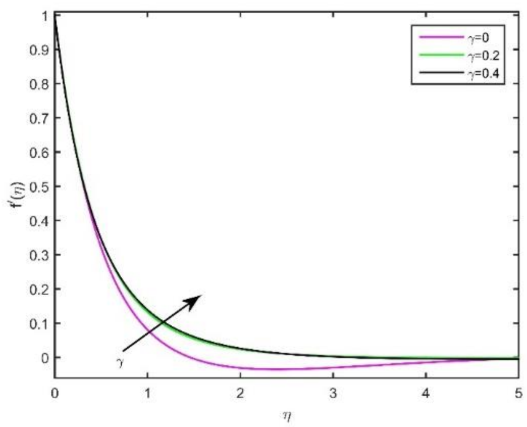

Figure 5. Effects of γ on the velocity profile.

As shown in Figure 5, the velocity f ′(η) increases as the curvature parameter (γ) increases. This indicates that higher curvature (γ) enhances the fluid flow along the vertically stretching cylinder, reducing resistance and thereby increasing the velocity of the ternary hybrid nanofluid within the porous medium. Figure 6 illustrates the impact of λ on fluid velocity, where it is noted that the velocity increases in tandem with increasing λ. This rise in λ bolsters the thermal buoyancy forces, consequently boosting the fluid's velocity and suggesting that buoyancy forces significantly accelerate fluid flow.

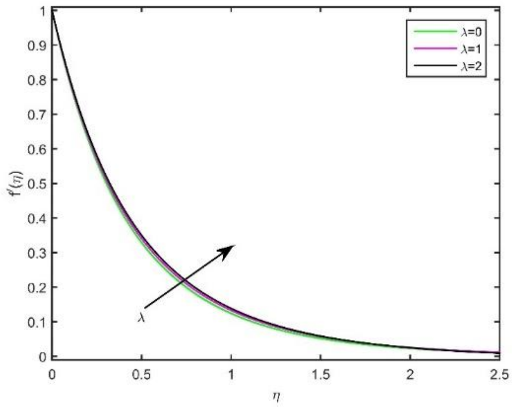

Figure 6. Effects of λ on the velocity profile.

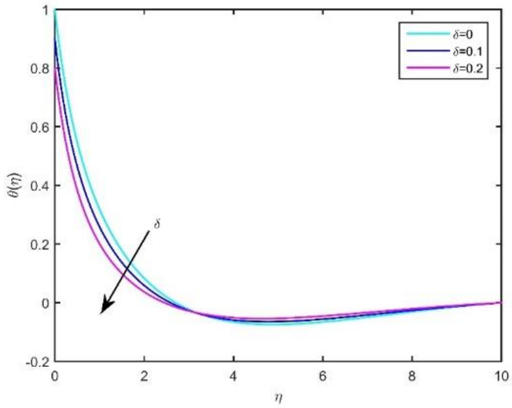

Figure 7. Effects of δ on the temperature profile.

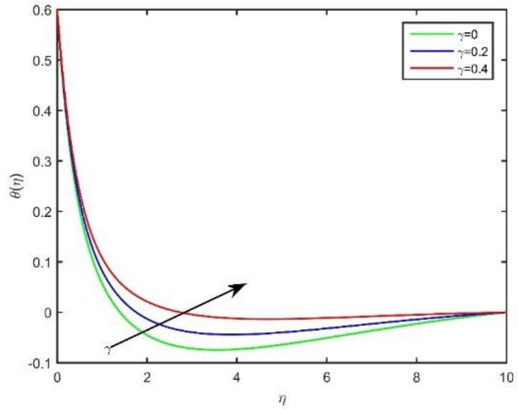

Figure 8. Effects of γ on the temperature profile.

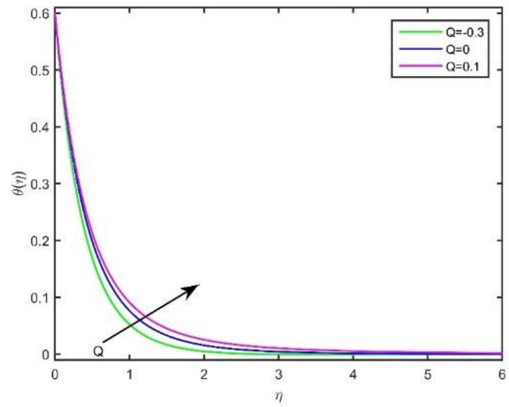

Figure 9. Effects of Q on the temperature profile.

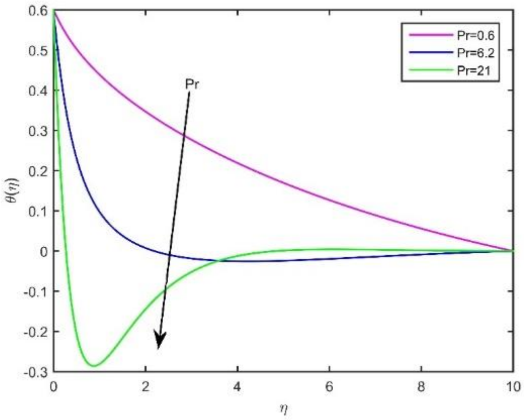

Figure 10. Effects of Pr on the temperature profile.

Figure 7 demonstrates that as thermal stratification (δ) rises, the fluid temperature declines. The presence of thermal stratification (δ) reduces the temperature gradient between the heated wall and the adjacent fluid, causing the thermal boundary layer to thicken and the temperature to decrease. Figure 8 shows that the temperature θ(η) increases as the curvature parameter γ increases. Higher curvature (γ) enhances thermal stratification, which leads to better thermal mixing and heat transfer within the fluid, thereby increasing the temperature. Figure 9 illustrates the result of the Q on the temperature profile, showing that as (Q) increases, the fluid temperature similarly rises, aligning with the fluid's fundamental physical properties. Figure 10 presents the effect of the P r on the fluid's temperature profile, revealing that an increase in Pr leads to a decrease in fluid temperature. A higher Pr suggests lower thermal conductivity, which reduces the efficiency of heat transfer through the fluid. Consequently, the rate of heat transfer diminishes, the thermal boundary layer narrows, and the fluid temperature decreases.

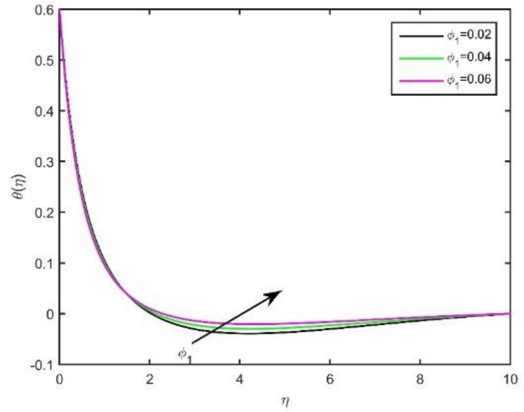

Figure 11. Effects of φ_1 on the temperature profile.

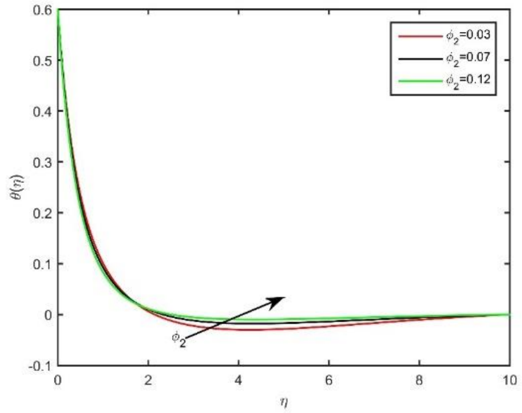

Figure 12. Effects of φ_2 on the temperature profile.

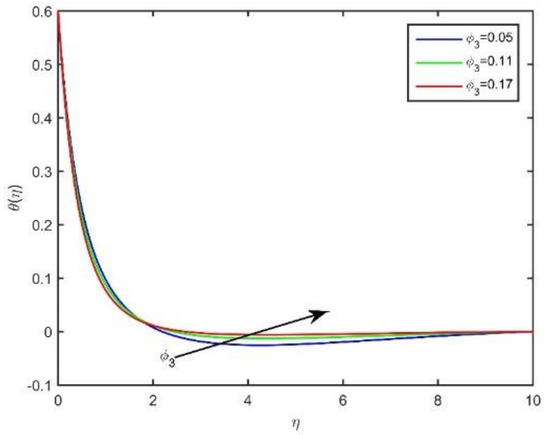

Figure 13. Effects of φ_3 on the temperature profile.

Figure 11 shows that a rise in the percentage of solid volume of Ag nanoparticles, with the volume fractions of $CoFe_2O_4$ and ZnO held constant, causes an increase in the temperature profile. Furthermore, Figure 12 demonstrates that the temperature increases as the percentage of the volume that $CoFe_2O_4$ rises while keeping the Ag and ZnO fractions constant. Similarly, an elevated volume fraction of ZnO (φ_3), as depicted in Figure 13, results in a higher temperature profile, indicating that increased concentrations of these nanoparticles improve the fluid's thermal properties.

Tables 3 detail the effects of various flow parameters on skin friction and the local Nusselt number. With a rise in the thermal stratification parameter (δ), skin friction and the local Nusselt number decrease. Higher values of the M and the K also lead to decreases in both skin friction and the Nusselt number. In contrast, increases in the value of λ result in higher skin friction friction and Nusselt number. For the Pr, while skin friction decreases, the Nusselt number increases. Similarly, a rise in the Q decreases the heat transfer rate, but skin friction increases. Lastly, as the γ increases, skin friction decreases, but the Nusselt number rises.

Table 3. Skin friction coefficient and local Nusselt number for different values of δ, M, K, λ, Pr, Q, γ.

δ	M	K	λ	Pr	Q	γ	Skin-friction coefficient	Local Nusselt number
0							-4.6237	2.6921
0.3	1.5	3	1.5	6.2	0.3	0.3	-4.7881	2.5381
0.5							-4.8867	2.3541
	0						-4.3195	2.5855
0.4	1.3	3	1.5	6.2	0.3	0.3	-4.6474	2.5132
	1.5						-4.9147	2.4446
		0					-3.2065	3.1715
0.4	1.3	2	1.5	6.2	0.3	0.3	-4.3406	2.5816
		4					-5.2901	2.3442
			0				-5.0461	2.3555
0.4	1.3	3	1	6.2	0.3	0.3	-4.9060	2.4280
			2				-4.7761	2.4975
				0.6			-4.6845	0.5110
0.4	1.3	3	1.5	6.2	0.3	0.3	-4.8399	2.4642
				21			-5.0492	6.5163
					-0.3		-4.8671	3.1050
0.4	1.3	3	1.5	6.2	0	0.3	-4.8531	2.7983
					0.1		-4.8456	2.6708
						0	-4.6327	2.9534
0.4	1.3	3	1.5	6.2	0.3	0.2	-4.7382	2.3769
						0.4	-4.9429	2.5709

Table 4. Comparison of skin friction coefficient.

δ	Nanofluid	Hybrid nanofluid	Ternary hybrid nanofluid
0.0	3.3154	4.2717	4.6237
0.1	3.3042	4.3242	4.6795
0.2	3.3552	4.3759	4.7345

Table 5. Comparison of local Nusselt number.

δ	Nanofluid	Hybrid nanofluid	Ternary hybrid nanofluid
0.0	2.8469	2.6112	2.6921
0.1	2.4314	2.5706	2.6484
0.2	2.394	2.5244	2.5983

Tables 4 and 5 present comparisons of the absolute skin friction and the local Nusselt number across nanofluid, hybrid nanofluid, and ternary hybrid nanofluid formulations. The ternary hybrid nanofluid ($Ag-CoFe_2O_4-ZnO/C_2H_6O_2+H_2O$) demonstrates a substantial enhancement in skin friction relative to the nanofluid ($Ag/C_2H_6O_2+H_2O$). Additionally, as thermal stratification (δ) increases, the disparity in skin friction between the ternary hybrid nanofluid and the standard nanofluid narrows for $-C_f Re_x^{1/2}$. The Nusselt number for the ternary hybrid nanofluid shows a significant improvement over that of the conventional nanofluid. Moreover, an increase in thermal stratification (δ) augments the difference in the Nusselt number between the ternary hybrid nanofluid and the regular nanofluid for $Nu_x Re_x^{-1/2}$.

5. Conclusions

An extensive study was conducted on the consequences of the thermal stratification effect regarding the movement of a ternary hybrid nanofluid that demonstrates magnetohydrodynamics characteristics through a vertically stretchable cylinder. This study considered the existence of a thermal buoyancy effect and a heat source within a porous medium. The study also looks at the flow features and how they affect temperature and velocity profiles, as well as the Nusselt number and friction factor. Notable findings from this inquiry include the following: As the parameters δ, K, and M grow, the velocity profile shows a decreasing trend while it shows a rising pattern with higher values of λ and γ. With rising values of δ and Pr, the temperature declines, whereas with rising values of φ_1, φ_2, φ_3, Pr, γ and Q, it rises. Parameters δ, M, K, Q, γ, and Pr cause a decrease in absolute skin friction, whereas λ causes it to increase. An upward trend is noted in the local Nusselt number as the values of Pr and γ increase, whereas a downward trend is observed as δ, M, K, λ, and Q increase. In comparison to the hybrid nanofluid, the ternary hybrid nanofluid exhibits higher absolute skin friction. Similarly, when compared to ordinary nanofluids, hybrid nanofluids exhibit higher skin friction. A ternary hybrid nanofluid has a greater heat transfer rate than a hybrid nanofluid, which is also higher than that of standard nanofluids.

Funding

This research received no external funding.

Acknowledgments

The authors have nothing to report.

Conflicts of Interest

The authors declare no conflict of interest.

References

1. Choi, S.U.S.; Eastman, J.A. ENHANCING THERMAL CONDUCTIVITY OF FLUIDS WITH NANOPARTICLES. Argonne National Lab.(ANL), Argonne, IL (United States): **1995**.
2. Das, S.; Jana, R.N. Natural convective magneto-nanofluid flow and radiative heat transfer past a moving vertical plate. *Alex. Eng. J.* **2015**, *54*, 55-64, https://doi.org/10.1016/j.aej.2015.01.001.
3. Das, S.; Jana, R.N.; Makinde, O.D. Transient natural convection in a vertical channel filled with nanofluids in the presence of thermal radiation. *Alex. Eng. J.* **2016**, *55*, 253-262, https://doi.org/10.1016/j.aej.2015.10.013.
4. Rashidi, M.M.; Momoniat, E.; Ferdows, M.; Basiriparsa, A. Lie Group Solution for Free Convective Flow of a Nanofluid Past a Chemically Reacting Horizontal Plate in a Porous Media. *Math. Probl. Eng.* **2014**, *2014*, 239082, https://doi.org/10.1155/2014/239082.
5. Abolbashari, M.H.; Freidoonimehr, N.; Nazari, F.; Rashidi, M.M. Entropy analysis for an unsteady MHD flow past a stretching permeable surface in nano-fluid. *Powder Technol.* **2014**, *267*, 256-267, https://doi.org/10.1016/j.powtec.2014.07.028.
6. Motsumi, T.G.; Makinde, O.D. Effects of thermal radiation and viscous dissipation on boundary layer flow of nanofluids over a permeable moving flat plate. *Phys. Scr.* **2012**, *86*, 045003, https://doi.org/10.1088/0031-8949/86/04/045003.
7. Turkyilmazoglu, M. Exact analytical solutions for heat and mass transfer of MHD slip flow in nanofluids. *Chem. Eng. Sci.* **2012**, *84*, 182-187, https://doi.org/10.1016/j.ces.2012.08.029.
8. Sahu, D.; Deka, R.K. Dynamic interaction of stratifications in a MHD parabolic flow with periodic temperature variation and variable mass diffusion in a porous medium. *International Communications in Heat and Mass Transfer. Part C*, **2024**, *159*, 108203, https://doi.org/10.1016/j.icheatmasstransfer.2024.108203.
9. Cheng, C.-Y. Double-diffusive natural convection along a vertical wavy truncated cone in non-Newtonian fluid saturated porous media with thermal and mass stratification. *Int. Commun. Heat Mass Transf.* **2008**, *35*, 985-990, https://doi.org/10.1016/j.icheatmasstransfer.2008.04.007.
10. Cheng, C.-Y. Combined heat and mass transfer in natural convection flow from a vertical wavy surface in a power-law fluid saturated porous medium with thermal and mass stratification *Int. Commun. Heat Mass Transf.* **2009**, *36*, 351-356, https://doi.org/10.1016/j.icheatmasstransfer.2009.01.003.
11. Sahu, D.; Deka, R.K. Thermal and Mass Stratification Effects on MHD Flow Past an Accelerated Vertical Plate with Variable Temperature and Exponential Mass Diffusion Embedded in a Porous Medium. *East Eur. J. Phys.* **2024**, 161-171, https://doi.org/10.26565/2312-4334-2024-2-15.

12. Sahu, D.; Deka, R.K. Thermal Stratification and Chemical Reaction Effects on MHD Flow Through Oscillatory Vertical Plate in a Porous Medium with Temperature Variation and Exponential Mass Diffusion. *East Eur. J. Phys.* **2024**, 209-218, https://doi.org/10.26565/2312-4334-2024-2-20.
13. Sahu, D.; Deka, R.K. Influences of thermal stratification and chemical reaction on MHD free convective flow along an accelerated vertical plate with variable temperature and exponential mass diffusion in a porous medium. *Heat Transfer* **2024**, *53*, 3643-3666, https://doi.org/10.1002/htj.23106.
14. Das, P.; Deka, R.K. Thermal and Mass Stratification Effects on Unsteady MHD Parabolic Flow Past an Infinite Vertical Plate with Variable Temperature and Mass Diffusion Through Porous Medium. *East Eur. J. Phys.* **2024**, 181-191, https://doi.org/10.26565/2312-4334-2024-2-17.
15. Nath, R.S.; Kumar, H.; Deka, R.K. Theoretical investigation of thermal and mass stratification effects on unsteady flow across a vertical oscillating plate with periodic temperature variation and variable mass diffusion. *Heat Transfer*. **2024**, *53*, 3605-3624, https://doi.org/10.1002/htj.23105.
16. Nath, R.S.; Deka, R.K. Theoretical Study of Thermal and Mass Stratification Effects on MHD Nanofluid Past an Exponentially Accelerated Vertical Plate in a Porous Medium in Presence of Heat Source, Thermal Radiation and Chemical Reaction. *Int. J. Appl. Comput. Math.* **2024**, *10*, 92, https://doi.org/10.1007/s40819-024-01721-9.
17. Sahu, D.; Deka, R.K. Influences of thermal and mass stratification on unsteady magnetohydrodynamics parabolic flow along an infinite vertical plate with periodic temperature variation and exponential mass diffusion in porous medium. *Heat Transfer*, **2024**, 53, 8, 4822-4850https://doi.org/10.1002/htj.23157.
18. Shanmugapriya, M.; Sundareswaran, R.; Senthil Kumar, P.; Rangasamy, G. Impact of nanoparticle shape in enhancing heat transfer of magnetized ternary hybrid nanofluid. *Sustain. Energy Technol. Assessments* **2022**, *53*, 102700, https://doi.org/10.1016/j.seta.2022.102700.
19. Arif, M.; Kumam, P.; Kumam, W.; Mostafa, Z. Heat transfer analysis of radiator using different shaped nanoparticles water-based ternary hybrid nanofluid with applications: A fractional model. *Case Stud. Therm. Eng.* **2022**, *31*, 101837, https://doi.org/10.1016/j.csite.2022.101837.
20. Patil, P.M.; Goudar, B.; Sheremet, M.A. Tangent hyperbolic ternary hybrid nanofluid flow over a rough-yawed cylinder due to impulsive motion. *J. Taibah Univ. Sci.* **2023**, *17*, 2199664, https://doi.org/10.1080/16583655.2023.2199664.
21. Mahmood, Z.; Iqbal, Z.; Alyami, M.A.; Alqahtani, B.; Yassen, M.F.; Khan, U. Influence of suction and heat source on MHD stagnation point flow of ternary hybrid nanofluid over convectively heated stretching/shrinking cylinder. *Adv. Mech. Eng.* **2022**, *14*, 16878132221126278, https://doi.org/10.1177/16878132221126278.
22. Cao, W.; I.L, A.; Yook, S.-J.; V.A, O.; Ji, X. Simulation of the dynamics of colloidal mixture of water with various nanoparticles at different levels of partial slip: Ternary-hybrid nanofluid. *Int. Commun. Heat Mass Transf.* **2022**, *135*, 106069, https://doi.org/10.1016/j.icheatmasstransfer.2022.106069.
23. Rupam Shankar, N.; Rudra Kanta, D. A Numerical Investigation of the MHD Ternary Hybrid Nanofluid (Cu-Al2O3-TiO2/H2O) Past a Vertically Stretching Cylinder in a Porous Medium with Thermal Stratification. *J. Adv. Res. Fluid Mech. Therm. Sci.* **2024**, *116*, 78-96, https://doi.org/10.37934/arfmts.116.1.7896.
24. Nath, R.S.; Deka, R.K. A Numerical Study on the MHD Ternary Hybrid Nanofluid (Cu-Al2O3-TiO2/H2O) in presence of Thermal Stratification and Radiation across a Vertically Stretching Cylinder in a Porous Medium. *East Eur. J. Phys.* **2024**, 232-242, https://doi.org/10.26565/2312-4334-2024-1-19.
25. Sarma, N.; Paul, A. Thermophoresis and Brownian Motion Influenced Bioconvective Cylindrical Shaped Ag–CuO/H_2O Ellis Hybrid Nanofluid Flow Along a Radiative Stretched Tube with Inclined Magnetic Field. *BioNanoScience* **2024**, *14*, 1266-1292, https://doi.org/10.1007/s12668-023-01280-1.
26. Paul, A.; Sarma, N.; Patgiri, B. Mixed convection of shear-thinning hybrid nanofluid flow across a radiative unsteady cone with suction and slip effect. *Mater. Today Commun.* **2023**, *37*, 107522, https://doi.org/10.1016/j.mtcomm.2023.107522.
27. Paul, A.; Sarma, N.; Patgiri, B. Thermal and mass transfer analysis of Casson-Maxwell hybrid nanofluids through an unsteady horizontal cylinder with variable thermal conductivity and Arrhenius activation energy. *Numer. Heat Transf.; A: Appl.* **2023**, 1-26, https://doi.org/10.1080/10407782.2023.2297000.
28. Shampine, L.F.; Kierzenka, J.; Reichelt, M.W. Solving Boundary Value Problems for Ordinary Differential Equations in Matlab with bvp4c. *Tutorial notes* **2000**, *2000*, 1-27.
29. Kierzenka, J.; Shampine, L.F. A BVP solver based on residual control and the Maltab PSE. *ACM Trans. Math. Softw.* **2001**, *27*, 299-316, https://doi.org/10.1145/502800.502801.

30. Paul, A.; Mani Nath, J.; Kanti DaS, T. An investigation of the MHD Cu-Al2O3/H2O hybrid-nanofluid in a porous medium across a vertically stretching cylinder incorporating thermal stratification impact. *J. Therm. Eng.* **2023**, *9*, https://doi.org/10.18186/thermal.1300847.
31. Paul, A.; Patgiri, B.; Sarma, N. Darcy-Forchheimer flow of Ag–ZnO–$CoFe_2O_4$/H_2O Casson ternary hybrid nanofluid induced by a rotatory disk with EMHD. *Int. J. Ambient Energy* **2024**, *45*, 2313697, https://doi.org/10.1080/01430750.2024.2313697.
32. Paul, A.; Sarma, N.; Patgiri, B. Numerical Assessment of MHD Thermo-mass Flow of Casson Ternary Hybrid Nanofluid Around an Exponentially Stretching Cylinder. *BioNanoScience* **2024**, 1-16, https://doi.org/10.1007/s12668-024-01306-2.
33. Hale, N.P. A Sixth-Order Extension to the MATLAB bvp4c Software of J. Kierzenka and L. Shampine. Master Degree, Imperial College London, London, England, **2006**.
34. Waini, I.; Ishak, A.; Pop, I. Mixed convection flow over an exponentially stretching/shrinking vertical surface in a hybrid nanofluid. *Alex. Eng. J.* **2020**, *59*, 1881-1891, https://doi.org/10.1016/j.aej.2020.05.030.
35. Ishak, A.; Nazar, R. Laminar boundary layer flow along a stretching cylinder. *Eur. J. Sci. Res.* **2009**, *36*, 22-29.
36. Elbashbeshy, E.M.A.; Emam, T.G.; El-Azab, M.S.; Abdelgaber, K.M. Laminar boundary layer flow along a stretching cylinder embedded in a porous medium. *Int. J. Phys. Sci.* **2012**, *7*, 3067-3072, https://doi.org/10.5897/JCECT11.087.